

https://doi.org/10.59887/2073-6673.2025.18(3)-9

EDN WLUNEY

УДК 551.46

© Yu. Yu. Yurovsky*, O. B. Kudinov, 2025

© Translated from Russian: Yu. Yu. Yurovsky, 2025

Marine Hydrophysical Institute RAS, 2 Kapitanskaya Str., Sevastopol, 299011, Russia

*y.yurovsky@mhi-ras.ru

Impact of Buoy Attitude Estimation Algorithms on Wave Parameter Retrieval: A Comparative Field Experiment

Received 31.03.2025, Revised 02.09.2025, Accepted 03.09.2025

Abstract

Microelectromechanical inertial sensors with embedded attitude determination algorithms have become standard in modern wave measurement buoys, though their proprietary nature often limits transparency in evaluating wave parameter accuracy. This paper presents the results of a field experiment with a prototype wave measuring buoy, in which raw triaxial accelerometer, gyroscope, and magnetometer data were recorded onto a memory card with minimal preprocessing. Subsequent post-processing was performed using various attitude estimation algorithms with open-source and easily accessible software implementations. The study examined both direct methods based on gravity and magnetic field measurements and more complex approaches, including the complementary filter and its variations (Mahony and Madgwick filters), as well as the Kalman filter and its extended version. The resulting attitude estimates enabled computation of both spectral wave characteristics and bulk parameters including significant wave height, peak period and mean direction. Comparative analysis against reference resistive wave gauge measurements revealed algorithm-dependent performance in the context of sea wave measurement. These findings offer practical insights for scenarios requiring either post-processing of raw buoy data or development of optimized embedded systems where full raw data transmission is not feasible.

Keywords: wave buoy, wave gauge, attitude heading reference system, wind waves, field study

© Ю. Ю. Юровский*, О. Б. Кудинов, 2025

© Перевод с русского: Ю. Ю. Юровский, 2025

Морской гидрофизический институт РАН, 299011, Севастополь, Капитанская ул., д. 2 *y.yurovsky@mhi-ras.ru

Влияние алгоритмов оценки ориентации волноизмерительных буев на восстанавливаемые параметры волн по данным сравнительного натурного эксперимента

Статья поступила в редакцию 31.03.2025, после доработки 02.09.2025, принята в печать 03.09.2025

Аннотация

Микроэлектромеханические инерциальные датчики со встроенными алгоритмами оценки ориентации широко применяются в современных волноизмерительных буях. Однако детали этих алгоритмов обычно скрыты от пользователя, что делает дальнейший анализ измерений характеристик волнения и их точность не совсем прозрачными. В данной работе представлены результаты натурного эксперимента с прототипом волноизмерительного буя, в котором измерения трёхосевых акселерометра, гироскопа и магнитометра записывались в максимально «сыром» виде на карту памяти. Последующая обработка проводилась с использованием различных алгоритмов оценки ориентации, имеющих открытую и легко доступную программную реализацию. В исследо-

Ссылка для цитирования: *Юровский Ю.Ю., Кудинов О.Б.* Влияние алгоритмов оценки ориентации волноизмерительных буев на восстанавливаемые параметры волн по данным сравнительного натурного эксперимента // Фундаментальная и прикладная гидрофизика. 2025. Т. 18, № 3. С. 114—128. EDN WLUNEY. https://doi.org/10.59887/2073-6673.2025.18(3)-9 For citation: Yurovsky Yu.Yu., Kudinov O.B. Impact of Buoy Attitude Estimation Algorithms on Wave Parameter Retrieval: A Comparative Field Experiment. *Fundamental and Applied Hydrophysics*. 2025;18(3):114—128. https://doi.org/10.59887/2073-6673.2025.18(3)-9

вании рассматривались как прямые методы оценки по измерениям силы тяжести и магнитного поля, так и более сложные подходы, включая комплементарный фильтр и его вариации (фильтры Махони и Маджвика), а также фильтр Калмана и его расширенную версию. Полученные разными способами оценки ориентации использовались для расчёта одномерных частотных и двумерных частотно-угловых спектров, а также для определения интегральных параметров волнения, таких как высота значительных волн, период волн, соответствующих пику спектра, и средневзвешенное направление волн. Результаты, полученные разными алгоритмами, сопоставлены с референтными измерениями, выполненными струнными волнографами. На основе этого сравнения сделаны выводы о качестве работы алгоритмов в контексте задачи измерения морских волн. Представленные результаты могут быть полезны как для постобработки исходных измерений волноизмерительных буев (как в данном исследовании), так и для разработки встроенных алгоритмов, в случаях, когда передача всего объёма исходных данных не представляется возможной.

Ключевые слова: волноизмерительный буй, волнограф, алгоритм оценки ориентации, ветровые волны, натурный эксперимент

1. Introduction

Hull-fixed inertial motion units (IMUs) are widely used in buoys designed to measure surface wave parameters (see e. g. [1]). Due to the absence of moving parts, such systems are significantly lighter, more compact, and orders of magnitude cheaper than mechanically stabilized alternatives. The main components of these IMUs are sensors that measure acceleration (accelerometers), angular velocity (gyroscopes), and magnetic field (magnetometers). Hereafter, these three types of sensors are collectively referred to as "inertial sensors".

It should be noted that velocity sensors based on Doppler measurements of global navigation satellite systems (GNSS) signals have recently been increasingly used in wave measuring buoys [2]. However, the use of inertial sensors alone remains relevant due to their advantages over GNSS sensors: lower average cost (~10 times for GNSS-sensors with Doppler channel), high noise immunity, lower power consumption, and no need for an external antenna. These features open broad prospects for using inertial sensors in the development of fleets (swarms) of simple, compact, and inexpensive measuring devices designed for specialized experimental studies of surface waves in field conditions (see e. g. [3]).

The lack of a mechanically stabilized platform in hull-fixed IMUs is also a drawback, as it necessitates referencing measurements to the world coordinates when calculating surface wave parameters — that is, estimating the buoy instantaneous attitude [4]. At first glance, such an estimate could be obtained by integrating gyroscopic measurements with given initial conditions. However, in practice, wave measurements without initial condition corrections must continue for several days, months, or even years, while gyroscope drift (and its variability due to external factors) makes such a direct attitude estimation impossible. Therefore, determining the current attitude requires assimilating (fusing) other measurements, such as geomagnetic field data (from magnetometers) and the gravity vector (from accelerometers). Yet, these measurements are also prone to errors. For example, the magnetic field can be distorted by the presence of magnetic materials, while gravity vector measurements can be affected by the sensor's own accelerations. While errors due to the former factor can be minimized by using non-magnetic materials, errors caused by the latter factor can be critical, as buoys continuously move with acceleration, replicating the orbital motion of waves. Nevertheless, the problem of estimating the attitude of a moving reference frame by assimilating various measurements is widespread in many applications [5]. Since the solution to this problem is non-unique, numerous algorithms of varying complexity, accuracy, and computational speed have been proposed to date ([6–16], discussed in more detail below).

Such algorithms are often embedded directly into the sensor controller (e. g., [17]). The user receives a ready-made attitude estimate, for example, in the form of Euler angles (roll, pitch, yaw) and accelerations in a fixed reference frame. Such IMUs are widely used in industry, unmanned systems, and robotics. Wave measuring buoys are no exception. The availability of such systems has enabled the development of buoys for studying ocean-atmosphere boundary layer processes [18], wave transformation in coastal zones [19], wave-ice interactions [1], satellite calibration [20] at relatively low costs.

However, attitude estimation algorithms are typically proprietary and not disclosed by manufacturers. The sensors themselves, with built-in algorithms, are usually designed for a wide range of tasks, raising questions about their optimality for surface wave measurements. For example, conventionally «slow» motions (with minimal influence from advective accelerations) are better reproduced by a combination of accelerometer and magnetometer measurements, while conventionally «fast» motions (with strong advective accelerations) can be more accurately reconstructed using gyroscope measurements [10]. However, it remains unclear which type of motion surface waves should be classified as in this context. It should be noted that commercial solutions specifically designed for wave buoys do exist (e. g., SVS-603HR [21], MOTUS [22], DVS19-2 [23]), but even in these cases, data processing algorithms are generally not disclosed. As a result, researchers are spared the need to delve deeply into the nuances of inertial navigation algorithms but are forced to use the measuring device as a "black box" which, in our view, is more of a drawback than an advantage.

The aim of this work is to demonstrate how the choice of a particular inertial data processing method affects the results of measuring various wave parameters. Within a single paper, it is impossible to examine in detail all the intricacies of numerical realization, perhaps, even for a single algorithm, let alone several. Therefore, this comparative analysis uses only easily accessible open-source algorithms. The input data consist of field measurements obtained using a prototype wave measuring buoy in which two different sensor models were installed at the closest possible distance. This setup also allowed us to assess how critical the choice of sensor model is for obtaining raw inertial measurements (excluding the influence of the processing algorithm).

2. Materials and Methods

2.1. Field Data

The study uses data from a field experiment conducted in 2024 at the Black Sea Hydrophysical Subsatellite Polygon near the Stationary Oceanographic Platform ($44.393047^{\circ}N$, $33.984596^{\circ}E$). During the experiment, continuous measurements were carried out using several prototype wave measuring buoys. This paper presents data from one of the buoys, which was anchored approximately 200 m from the platform at a depth of ~27 m.

The buoy operates as a logger, collecting inertial measurements and storing it on a memory card without preprocessing. The sampling rate is 25 Hz, the memory card capacity is 32 GB, and power is supplied by six lithium-ion batteries with a total capacity of 50 Wh. The prototype is also equipped with a real-time clock, enabling synchronization of measurements with universal time. For methodological purposes, two "consumer-grade" IMUs of different models were installed in this prototype: the MPU-9250 [24] and the BNO-055 [17]. Both sensors measure three components of acceleration (gravity vector), angular velocity, and magnetic field. Additionally, the BNO-055 has an embedded data processing algorithm, and its output parameters (Euler angles) were also recorded on the memory card and later compared with the results of other processing algorithms during data analysis. The presence of two sensors from different manufacturers allows for a rough estimate of the variation in their parameters, as well as an assessment of the impact of their intrinsic uncorrelated noises.

The electronic components are housed in a sealed cylindrical enclosure with a diameter of 10 cm and a height of 30 cm, mounted inside a foam polystyrene float shaped like a disk (40 cm in diameter and 10 cm in height). The IMUs are aligned along the vertical axis of symmetry on opposite sides of the motherboard, ensuring minimal separation between them (in practice, they are horizontally offset by no more than 4 mm). Both sensors lie in the same horizontal plane, coinciding with the waterline plane — i. e., as close as possible to the point around which the buoy natural oscillations occur. To minimize the impact of sudden jolts caused by interactions between the buoy hull and steep/breaking waves [25], an elastic cord (a 7-m-long, 6-mm-diameter latex cord in a nylon sheath) was incorporated into the mooring line.

As reference ground truth, data from an array of string resistive wave gauges were used, enabling the acquisition of two-dimensional frequency-directional wave spectra [26]. Additionally, meteorological sen-

sors from a Davis Vantage Pro weather station were installed on the platform mast at a height of 21 m above sea level, including a cup anemometer, a wind vane for wind direction, and air temperature and humidity sensors. These data were later used to adjust wind speed to the standard 10-m height using the COARE3.0 algorithm [27].

A total of approximately one week (165 hours) of continuous measurements was collected (Fig. 1). During this period, wind speeds varied from 0 to 15 m/s, with shifting directions — predominantly easterly or westerly — over 1–3-day intervals. As a result, the waves in the observation area exhibited diverse directions, heights, and ages. The maximum significant wave height reached ~ 1 m, while the spectral peak frequency during the most intense wave conditions was ~ 0.2 Hz, which is typical for this site. Swell from the southeast was present for nearly the entire observation period, with a period of ~ 10 s and varying intensity. Thus, the wave conditions during the analyzed time interval can be characterized as highly diverse, which, in our opinion, enhances the representativeness of the presented analysis.

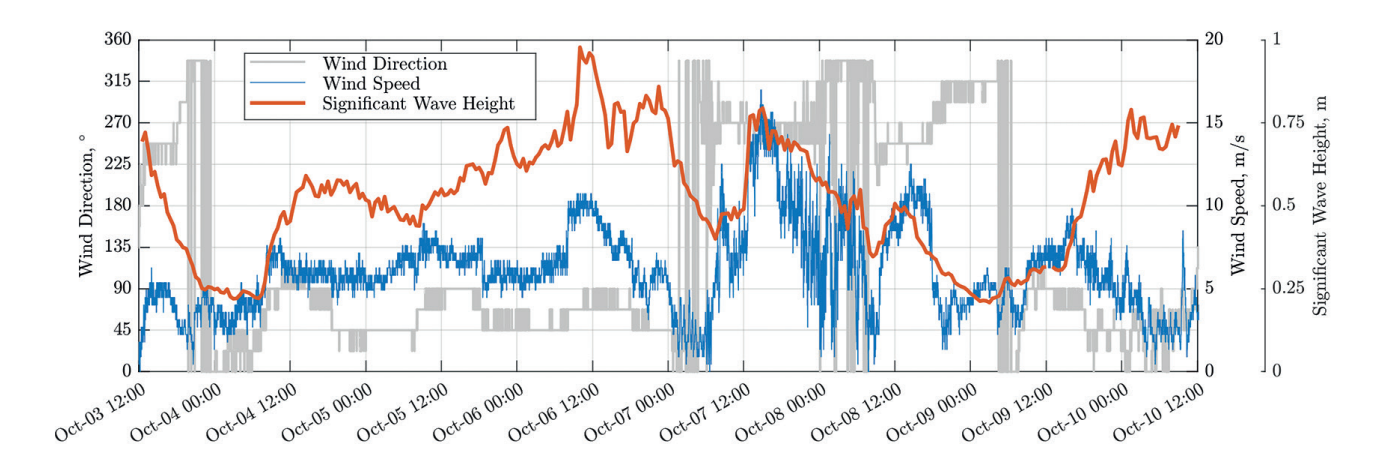


Fig. 1. Wind direction, wind speed, and significant wave height during the experiment

2.2. Attitude Estimation Algorithms

Attitude estimation of the buoy involves finding the rotation transformation from the moving coordinate system (associated with the buoy) to the fixed (world) reference frame. The algorithms used in this work can be conditionally divided into two groups. The first group includes algorithms that use only reference vector measurements as input data — the gravity vector (accelerometer measurements) and magnetic field (magnetometer measurements):

- TRIG/TRIM, TRI-axial Attitude Determination (TRIAD method). One of the earliest and simplest attitude estimation methods using observations of two non-collinear reference vectors [6]. When the vectors remain constant in both the moving and fixed reference frames, the method provides an exact solution in the form of a rotation matrix composed from vector triads. Real measurements always contain errors, thus the rotation transform aligns only one (priority) vector depending on the order of reference vectors used to construct the triads. In our notation, TRIG and TRIM indicate priority given to the gravity vector and magnetic field vector, respectively.
- DAVQ, Davenport's Q-method. This method involves finding eigenvalues and eigenvectors of a specially constructed matrix (Davenport's matrix) [7]. The optimal attitude quaternion corresponds to the eigenvector associated with the largest eigenvalue of this matrix.
- FLAE, Fast Linear Attitude Estimator. The method reduces the attitude estimation problem to linear equations based on quaternions and using pseudoinverse matrices [8], allowing attitude estimation through an eigenvalue-based solution while providing higher computational speed compared to DAVQ.

The second group comprises algorithms that utilize not only gravity and magnetic field measurements but also angular velocity measurements of the moving reference frame (gyroscope readings):

- ROLQ, Recursive Optimal Linear estimator of Quaternion. This approach employs optimal quaternion estimation via least squares with recursive incorporation of angular velocity measurements to suppress noise caused by potential distortions of the magnetic field and gravity vector due to inertial forces [9].
- COMF, Complementary Filter. This filter estimates attitude using gyroscope measurements and corrects it by fusing gravity and magnetic field measurements with specified weighting [10].
- MAHO, Mahony Filter. A variant of the complementary filter specifically developed for consumer-grade inertial sensors, featuring enhanced robustness against measurement channel noise [11]. The attitude estimate is corrected at each step by introducing a control (correction) angular velocity.
- MADG, Madgwick Filter. Similar to the Mahony filter, it's designed for sensors with distorted measurements [12]. Instead of angular velocity correction, it employs optimal quaternion correction obtained through gradient descent optimization.
- KALM, Kalman Filter. One of the most widely used filters across various scientific and engineering fields for predicting the state of dynamic systems while accounting for statistics of noisy and/or incomplete measurements [13].
- EKAF, Extended Kalman Filter. Unlike the standard linear Kalman filter, this method accounts for non-linearities in the dynamic system state prediction model and the consequent non-gaussianity of predicted variable distributions [14].

The study used numerical implementations of these algorithms with open-source code, available as ready-made toolboxes in MATLAB [15] (for COMF and KALM) and modules in Python [16] (for all others). The filters listed in the second group, with the exception of the ROLQ method, have configurable parameters. For complementary filters, these are the weights of correction estimates based on magnetometer and gyroscope readings. For the Kalman filter, these are the noise variances of measurement channels (their values are close to those of the sensors used). This work used the "default" values set in the source codes. To avoid potential confusion in axis definitions, the algorithm functionality was preliminarily tested on simple model data and laboratory experiments (rotations around the sensor axes relative to geographic axes and accelerated movements along them).

In addition, the results from the built-in algorithm of the BNO-055 sensor (denoted as BSCH) were used. Additionally, data without vertical correction (denoted as NONE) were considered under the assumption that vertical accelerations in the moving and fixed coordinate systems are the same (applicable only for wave heights and periods, since wave direction estimation is not defined in this case).

2.3. Wave Parameter Estimates

The directional wave spectrum is estimated from measurements of vertical accelerations and hull tilt angles using the classical Longuet-Higgins method [28], where the wave elevation spectrum is represented as a truncated Fourier series:

$$S(f,\theta) = \frac{a_0}{2} + \sum_{n=1}^{2} (a_n \cos n\theta + b_n \sin n\theta) = S_z(f)D(f,\theta), \tag{1}$$

where f is the frequency, $S_z(f)$ is the one-dimensional frequency elevation spectrum, $D(f, \theta)$ is the directional spreading function over the azimuth angle, θ (in our notations $\theta = 0$ corresponds to the waves coming from the north), n is the order of the coefficients in the Fourier expansion.

As shown in [28], measurements of accelerations and tilts are contained only in terms of order $n \le 2$. The corresponding coefficients a_0 , a_1 , a_2 , b_1 , and b_2 are computed from co- and cross-spectra of vertical acceleration and hull tilt angles (see a detailed description of this method in Section 3.2 of [29]).

A similar method was applied for processing string wave gauge data, with the difference that surface tilts were determined from the normal to the plane approximating instantaneous elevation measurements.

The significant wave height was determined through the zeroth moment of the elevation spectrum:

$$H_{\rm s} = 4 \cdot \left[\int_{f_{\rm l}} S_z(f) df \right]^{1/2},\tag{2}$$

where the elevation spectrum, S_z , is computed from vertical acceleration spectrum, S_a , as $S_z = \omega^{-4}S_a$, where $\omega = 2\pi f$ is the radial frequency. Due to the singularity at $\omega \to 0$, integration in (2) did not start from zero frequency but rather from frequency f_1 corresponding to the first local minimum of the elevation spectrum [3].

The spectral peak period was estimated via the first moment of the elevation spectrum using the method [30], which makes the conventional peak frequency estimate less dependent on spectral resolution,

$$T_{\rm p} = \left[\frac{\int_{f_1} f S_z(f)^4 df}{\int_{f_1} S_z(f)^4 df} \right]^{-1}.$$
 (3)

The mean-weighted wave direction was calculated as the spectrum-weighted average value [31]:

$$\Theta = \frac{\int_{f_1} \theta_1 S_z(f) df}{\int_{f_2} S_z(f) df},\tag{4}$$

where $\theta_1 = \arctan(b_1/a_1)$ is the frequency-dependent mean wave direction [29].

3. Results

The presence of two closely positioned sensors in a single buoy provides a clear demonstration of the magnitude of errors associated with random variations in specification scale factors or, as in our case, differences between sensor models from different manufacturers. To illustrate this, Fig. 2 shows the coherence and spectral ratios between the most important measurements used for wave parameter estimation: vertical accelerations, which are used to estimate the one-dimensional spectrum and consequently wave height and period (left); horizontal components of the magnetic field vector (center) and rotation rates around horizontal axes (right), which play a key role in reconstructing wave slopes, angular distribution spectral function, and estimating wave directions. The figure presents three most typical scenarios at wind speeds ~5 m/s, ~10 m/s, and ~15 m/s (indicated by different colors).

In all cases, an extremely high coherence level (\sim 0.99) is observed in the frequency range from the spectral peak (0.15...0.2 Hz) to the cutoff frequency (approximately 1 Hz for utilized hull). This indicates that measurements from both sensors primarily contain the wave-induced signal, while intrinsic noise contributes insignificantly. Notably, coherence remains relatively high (0.8...0.9) even at frequencies below the peak frequency, suggesting that the signal at these frequencies — an artifact known as low-frequency noise — is mainly caused by buoy motion rather than sensor instrumental noise. Slightly lower coherence below the peak frequency is observed under low wind conditions for rotation rates about the x-axis (dominant waves cause rotation about the y-axis). Nevertheless, even in this case, the coherence value remains no less than 0.7.

The spectral power ratio of vertical acceleration components between the two sensors (Fig. 2d) is close to unity, ranging between 0.95...1.05. Magnetic field and rotation rate measurements (Fig. 2e, f) show somewhat greater differences, with ratios of 0.90...1.05 (except for the aforementioned low wind case). The corresponding amplitude ratios represent variations of ~ 2.5 % and ~ 5 % respectively, well within the specified scale factor errors for these sensors (a few percent). We should note that for the magnetic field, where the greatest variations are observed, the absolute value is not crucial for slope estimation, only the vector direction matters. Below, unless comparing the two sensors directly, we will use MPU-9250 sensor measurements.

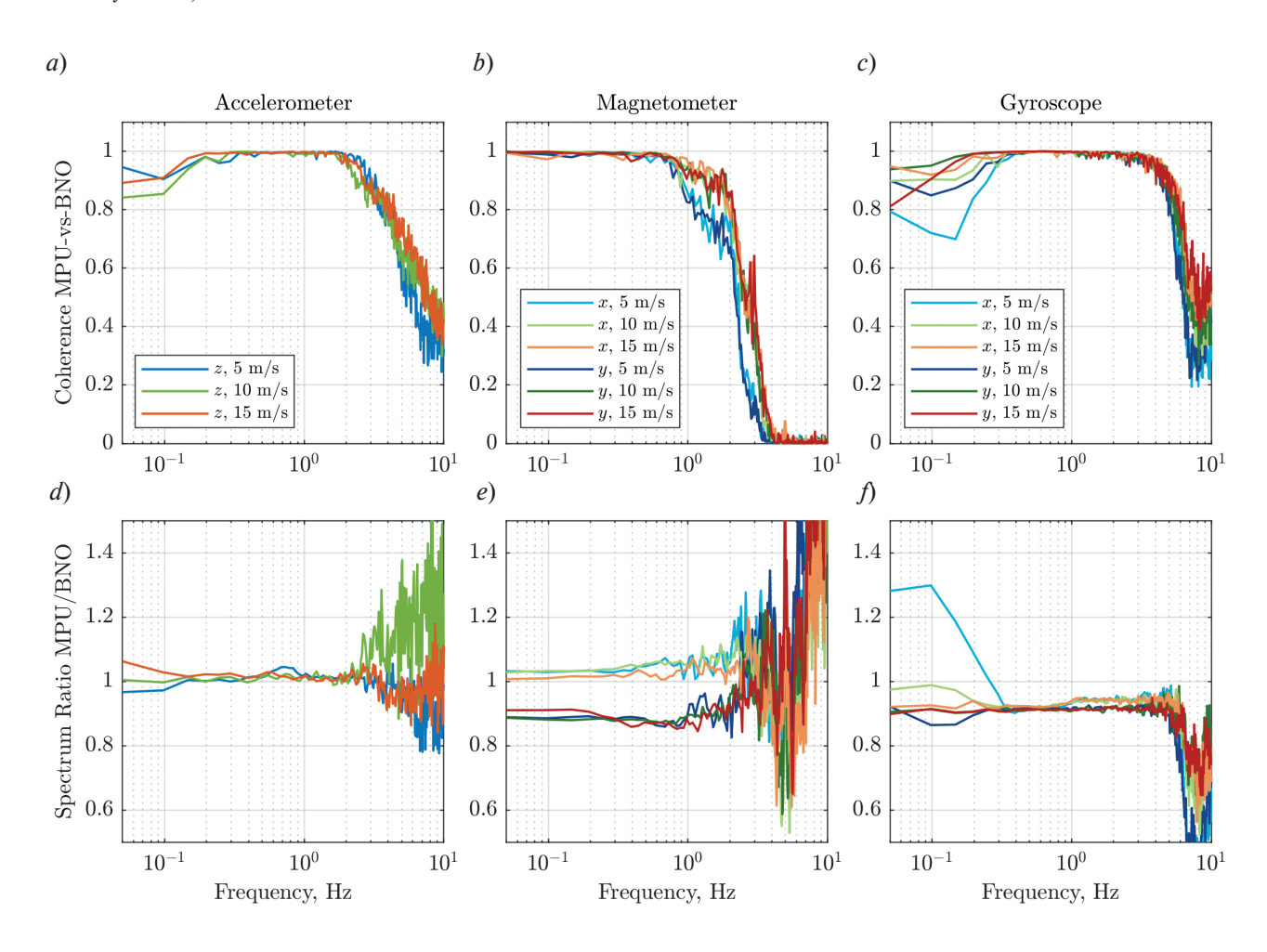


Fig. 2. Coherence (top) and spectral ratio (bottom) between raw measurements of the vertical accelerometer component (left), horizontal magnetometer components (middle), and gyroscope components (right) for MPU-9250 and BNO-055 sensors. Wind speed is color-coded: blue shades — 5 m/s (data from 07:00–08:00 on 04.10.2024), green shades — 10 m/s (10:00–11:00 on 06.10.2024), red shades — 15 m/s (15:00–16:00 on 07.10.2024)

Fig. 3 demonstrates an example of raw data processing using various attitude estimation algorithms, including reconstructed hull tilt angles, vertical accelerations, and sea surface elevations at ~10 m/s wind speed. The elevations were obtained by integrating accelerations after preliminary low-frequency component filtering using a filter with time constant corresponding to frequency f_1 .

The most significant differences between algorithms are observed in the estimates of hull tilt angles. While the estimates are generally similar, the average variation ranges from 5...10°. The exception are rare events (presumably wave breaking moments, as they correspond to spikes in all signals) where differences reach 20...40° and estimates may become anti-phase. The corresponding discrepancies in surface elevations reach 0.5 m, representing about half of the significant wave height. Thus, algorithm selection becomes critically important when analyzing individual waves, such as abnormally large waves or so-called rogue waves.

For regular (non-breaking) waves, differences between algorithms are less significant since tilt angles only introduce corrections to accelerations and elevations. However, fundamental differences appear in the low-frequency region, which is important for proper selection of the lower integration limit f_1 in (2). Fig. 3 shows an example of elevation spectra (in both logarithmic and linear scales), demonstrating that in the operational frequency range above the peak frequency the differences are minimal, while at low frequencies the spectral level difference reaches approximately an order of magnitude.

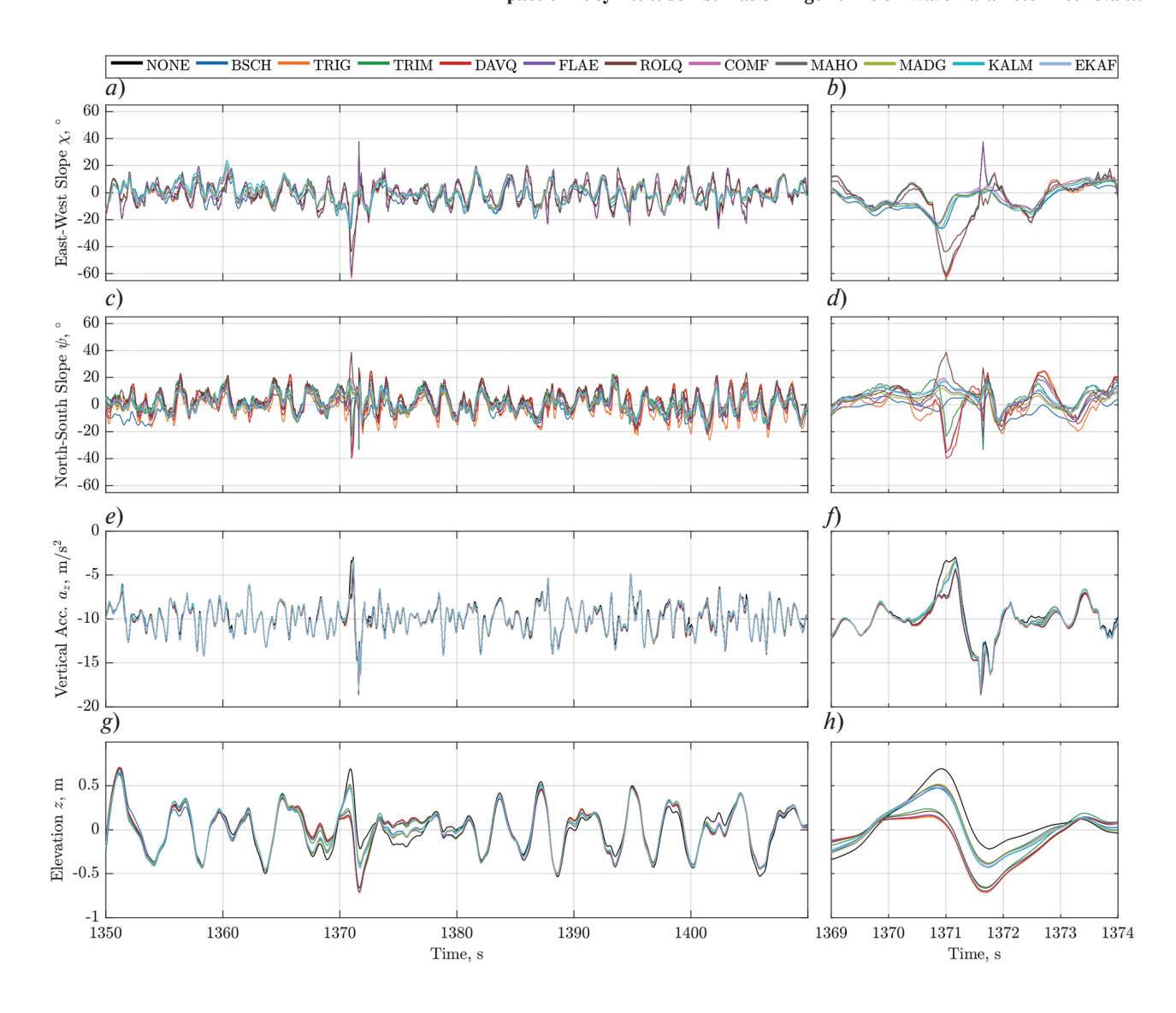


Fig. 3. Example of buoy motion reconstruction at 10 m/s wind speed from MPU-9250 sensor data: (a, b) hull tilt in west-east direction; (c, d) tilt in north-south direction; (e, f) vertical accelerations; (g, h) sea surface elevations. Left panels display a one-minute recording segment, right panels show a detailed section with a spike recorded at 1370 s

A more comprehensive evaluation of algorithm performance is presented in the diagram (Fig. 4c), showing the ratio of estimated to reference significant wave heights as a function of low-frequency noise level. The best results are demonstrated by KALM, EKAF, COMF, MAHO, MADG and BSCH algorithms (group in the lower left corner). Direct estimation algorithms (TRIG, TRIM, DAVQ, FLAE) exhibit ~3 times higher noise levels, though TRIM shows accuracy comparable to KALM, MAHO, MADG. The recursive ROLQ filter does not improve estimates and has an average signal-to-noise ratio close to 1 due to strong outliers in time series.

Despite these differences, it should be noted that all algorithms show good agreement with reference data in estimating significant wave height (deviations do not exceed 4...7.5 % for all algorithms). Selecting an optimal algorithm based on this criterion is hardly possible, as the measurement error of the reference wave gauge is of similar magnitude (comparable to the accuracy of the wave gauge calibration coefficients). Comparison of results from different sensors (visualized by the distance between points on the diagram) shows that the choice of sensor has significantly less impact on estimation accuracy than the choice of processing algorithm.

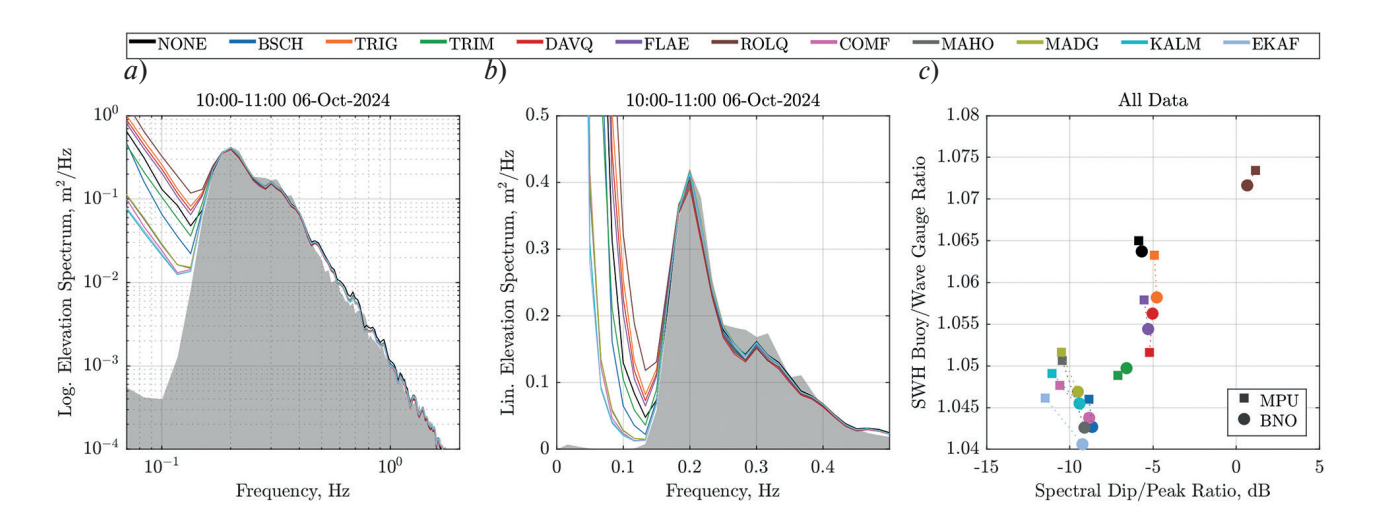


Fig. 4. Typical sea surface elevation spectrum at 10 m/s wind speed: a— spectral density in logarithmic scale; b— the same in linear scale. Colored curves represent estimates from MPU-9250 sensor measurements using different algorithms, while gray shading indicates reference wave gauge measurements. Panel c shows the dependence of the mean relative error in significant wave height estimation on the level of low-frequency noise (normalized to the spectrum's maximum value) for both MPU-9250 and BNO-055 sensors

The results of integral wave parameter estimation are more clearly presented in Fig. 5. The plots show time series of significant wave height H_s , peak wave period T_p , and mean-weighted wave direction Θ compared with reference wave gauge measurements (left panels), along with corresponding scatter plots (right panels).

The best agreement is observed for H_s parameter, with results showing practically no dependence on the chosen processing algorithm (Fig. 5 a, b). Only a slight systematic overestimation is noted for the time interval of October 7–9, when strong currents were observed in the study area. However, detailed analysis of this effect falls beyond the scope of the present study.

Significantly greater differences between algorithms are observed in peak period $T_{\rm p}$ estimates (Fig. 5 c, d). The time series show well pronounced outliers, most noticeable around midnight on October 4 and noon on October 9. These artifacts stem from errors in estimating frequency $f_{\rm l}$ and the influence of low-frequency noise. When overestimated, the true spectral peak becomes masked by low-frequency interference, while underestimated cases identify the swell peak instead of the main peak, artificially amplified by low-frequency noise. The highest frequency of such errors is characteristic of the ROLQ algorithm, which demonstrates the maximum level of low-frequency interference.

The most challenging situation occurs when estimating mean wave direction Θ (Fig. 5 e, f). Kalman filters (KALM, EKAF), complementary filters (COMF, MAHO, MADG), and the built-in BSCH algorithm provide stable estimates that closely match reference values. In contrast, direct estimation algorithms (TRIG, TRIM, DAVQ, FLAE, ROLQ) produce excessively noisy results, indicating their limited effectiveness for determining wave directional characteristics.

More detailed quantitative metrics for this comparative analysis are presented in Fig. 6 as diagrams simultaneously displaying both correlation coefficient (CC) and root mean square error (RMSE) between time series of H_s , T_p , and Θ obtained from both buoy measurements and reference wave gauge data.

When analyzing significant wave heights (Fig. 6 a, d), all algorithms except ROLQ show a slight but consistent improvement in estimates compared to the non-corrected version. Regardless of the algorithm or sensor choice, the correlation coefficient (CC) remains no less than 0.97, while the root mean square error (RMSE) typically ranges between 4.5...5.5 cm.

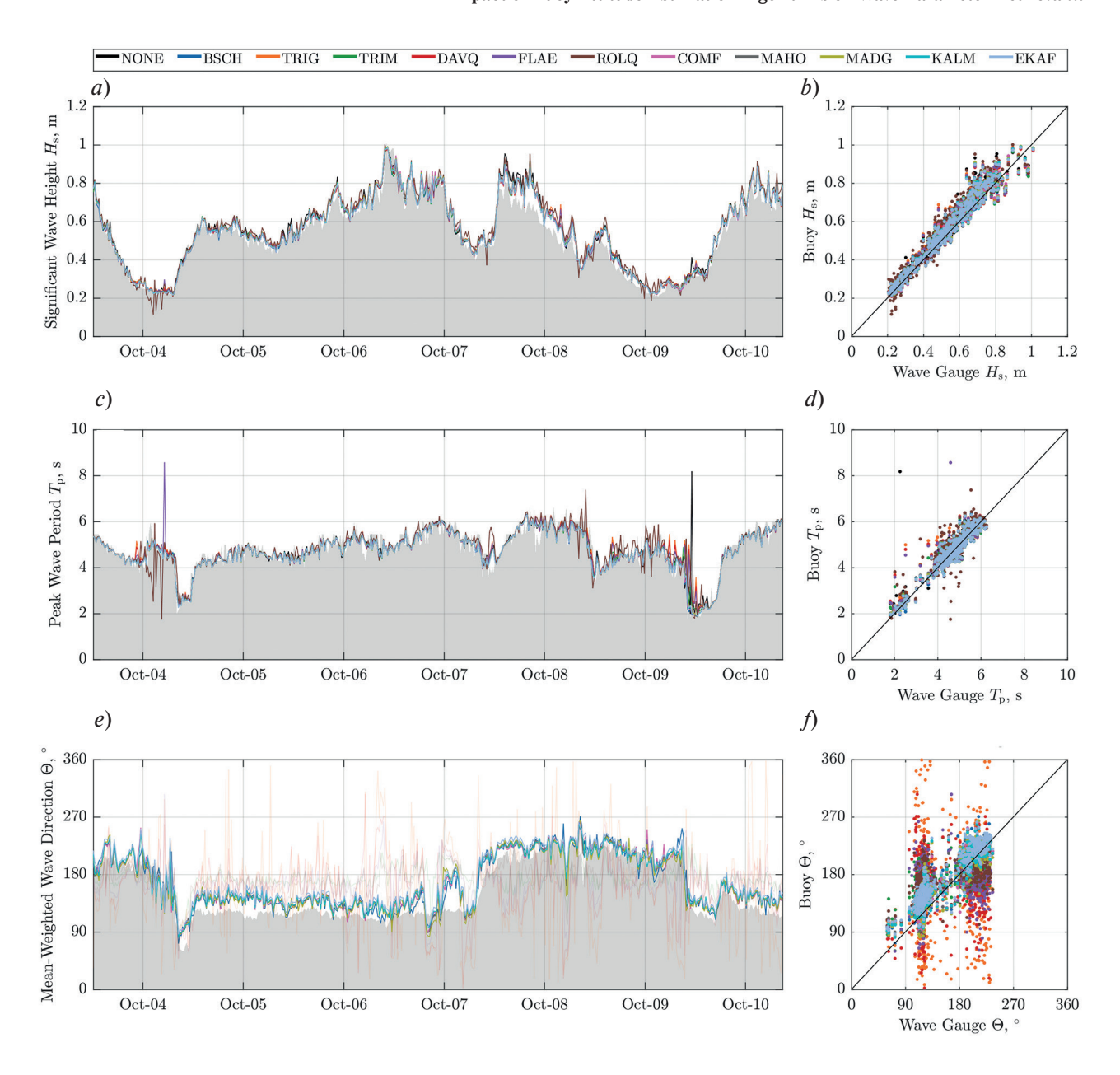


Fig. 5. Time series of significant wave height (a), peak wave period (c), and mean-weighted wave direction (e) from MPU-9250 sensor measurements using different color-coded estimation algorithms compared with reference wave gauge measurements (gray shading). The right panels (b, d, f) show corresponding scatter plots of estimates versus reference

For mean-weighted wave periods Θ (Fig. 6 b, e), a similar pattern is observed. The KALM, EKAF, COMF, MAHO, MADG and BSCH algorithms produce practically identical estimates, appearing as a single point on the diagrams with a correlation coefficient of ~0.95 and RMSE of ~0.25...0.35 s. Slightly less accurate results are shown by the TRIG, TRIM, DAVQ and FLAE algorithms, though they still provide improvement compared to no vertical correction.

In the case of wave directions (Fig. 6 c, f), the KALM, EKAF, COMF, MAHO, MADG and BSCH algorithms demonstrate good accuracy ($CC\sim0.90...0.94$, RMSE $\sim20^\circ$). The ROLQ algorithm shows poorer results ($CC\sim0.6$, RMSE $\sim40^\circ$), while the direct estimation methods TRIG, TRIM, DAVQ and FLAE fail to provide statistically significant results ($CC\sim0$).

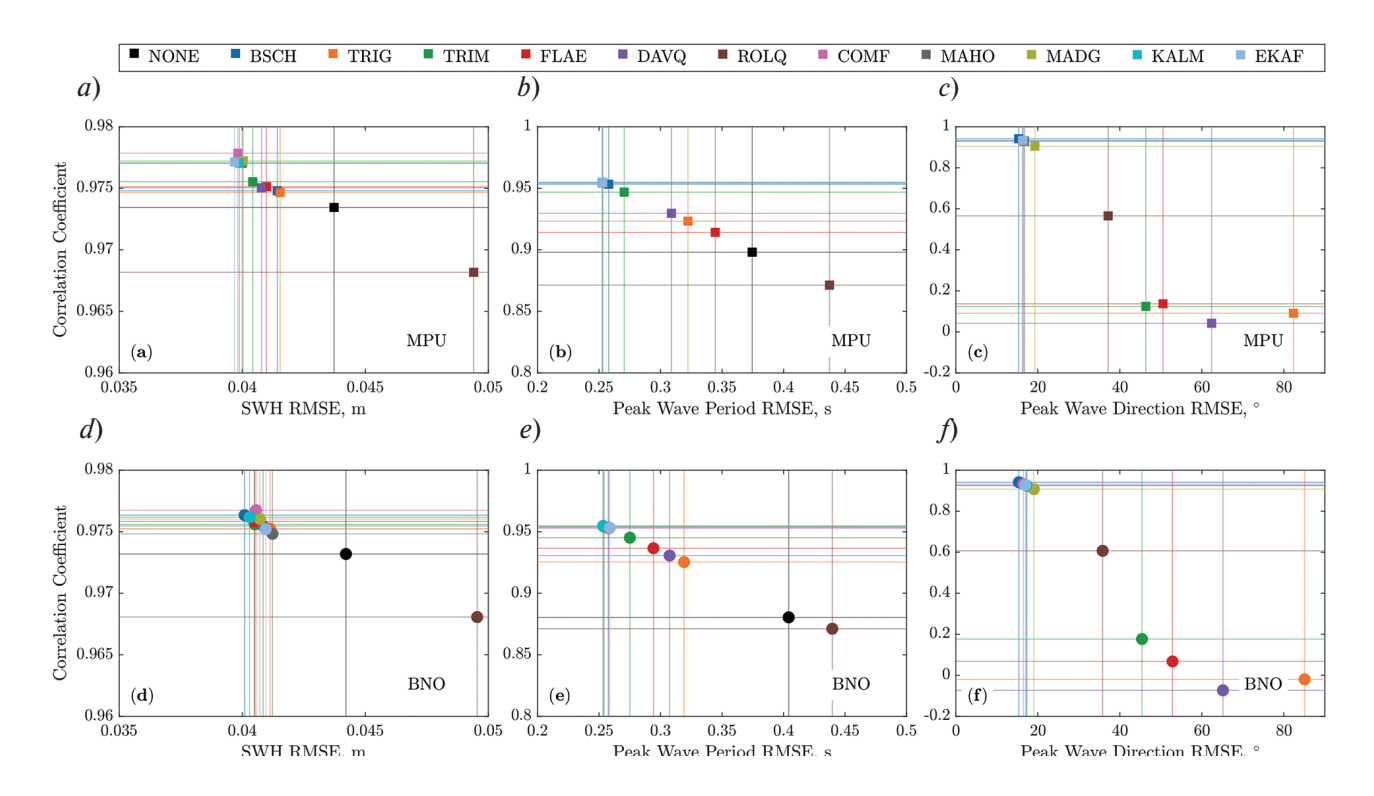


Fig. 6. Statistical indicators of wave parameter estimation accuracy: significant wave height (a, d), spectral peak wave period (b, e), and mean-weighted direction (c, f), presented in "correlation coefficient — root mean square error". The top row corresponds to measurements from the MPU-9250 sensor, while the bottom row shows results from the BNO-055 sensor

4. Discussion

It should be separately noted that the identified patterns may not be fully applicable to other buoys. Specifically, for miniature buoys designed to study the short-wave part of the spectrum, the use of the Kalman filter (KALM) may produce more noisy low-frequency spectra compared to the TRIAD method with magnetic field priority (TRIM) [32]. As shown in [3], low-frequency noise in the Kalman filter output may be caused by impulse noise at its input resulting from wave breaking. Small and lightweight buoys are significantly more sensitive to such events than large and heavy ones. Moreover, small-scale breaking is always more probable than large-scale breaking [33], which may reduce the effectiveness of Kalman-based algorithms under conditions of strong breaking-induced noise. Nevertheless, the filters that showed the best results in our study (KALM, EKAF, COMF, MAHO, MADG) have tuning capabilities. This work used default algorithm parameters, but their further optimization and adaptation to the characteristics of small buoys requires additional research efforts beyond the scope of this study.

Given the uncertainty that may arise from the choice of attitude estimation method, transferring this processing stage to shore-based systems, as implemented in our experiment, appears promising. This approach preserves maximum data volume and enhances transparency in subsequent data processing. The development of communication channels, increased computing power, and expanded data storage capacities further facilitate this concept. For example, a sensor with a sampling rate of 5 Hz (9 channels at 2 bytes per sample) requires ~3 GB of memory to store one year of observation data. The daily data transmission volume in this case does not exceed 8 MB, which is quite feasible using modern mobile networks, as demonstrated in [3]. Additional energy costs for data transmission can be partially offset by abandoning computationally expensive attitude estimation algorithms and, consequently, any other preprocessing. Such an operational scheme appears justified for coastal studies where mobile networks are available. For satellite communication channels in the open ocean, this approach is currently less effective due to high data transmission costs but may become promising in the future.

5. Conclusion

This study demonstrates how the selection of attitude estimation algorithms for wave measurement buoys influences the wave parameter retrieval, including one-dimensional frequency spectra and their spectral peak identification, as well as integral wave characteristics — significant wave height, peak period, and mean-weighted wave direction.

The analysis utilized open-source, easily accessible software implementations of attitude estimation algorithms [29,30], particularly methods based on direct estimation using gravity and magnetic field vectors (TRIAD-method, Davenport's Q-method, Fast Linear Attitude Estimator), complementary filters and their variants (Recursive Optimal Linear estimator of Quaternion, Mahony filter, Madgwick filter), Kalman filter and its so-called extended version. These algorithms were tested on field measurements using a prototype buoy that recorded raw accelerometer, gyroscope and magnetometer measurements for subsequent shore-based processing. Measurements from resistive wave gauges on a stationary oceanographic platform were used as reference ground truth.

The buoy was specially equipped with two closely located inertial sensors of the same price range, operating on similar physical principles but produced by different manufacturers (a combined accelerometer/gyroscope/magnetometer MPU-9250 [24] and BNO-055 [17]). The signals from these sensors showed high coherence and similar spectral composition, indicating minimal influence of their internal characteristics (noise and calibration coefficient variations) on the final derived wave parameters.

The results show that the choice of inertial data processing algorithm does not significantly affect the relative error in elevation spectrum measurements near the peak frequency (and consequently, significant wave height), but becomes crucial for spectral peak identification and low-frequency noise suppression. The largest errors occur under conditions of weak and mixed sea states. For retrieving wave direction, algorithms incorporating all sensor data (complementary filter variants and Kalman filters) prove most effective. In contrast, direct estimation methods relying solely on gravity and magnetic field vectors fail to provide reliable wave direction estimates when using conventional methods for determining two-dimensional spectra.

These findings can be valuable both for post-processing raw wave buoy measurements (shore-based, as in this study) and for developing algorithms performing onboard data processing in wave measuring systems when transmitting the full volume of raw data is impractical or impossible.

Funding

The research was supported by the Russian Science Foundation, grant No. 24-27-00153.

References

- 1. Rabault J, Nose T, Hope G, et al. OpenMetBuoy-v2021: an easy-to-build, affordable, customizable, open-source instrument for oceanographic measurements of drift and waves in sea ice and the open ocean. *Geosciences*. 2022;12(3):110. https://doi.org/10.3390/geosciences12030110
- 2. Collins CO, Dickhudt P, Thomson J, et al. Performance of moored GPS wave buoys. *Coastal Engineering Journal*. 2024;1–27. https://doi.org/10.1080/21664250.2023.2295105
- 3. Hope G, Seldal TI, Rabault J, et al. SFY a lightweight, high-frequency, and phase-resolving wave buoy for coastal waters. *Journal of Atmospheric and Oceanic Technology*. 2025;42(2):133—154. https://doi.org/10.1175/JTECH-D-23-0170.1
- 4. Gryazin DG. Calculation and design of buoys for sea wave measurements. St. Petersburg: SPbGU ITMO; 2000. 134 p. (in Russian).
- 5. Matveev VV, Raspopov VYa. Fundamentals of strapdown inertial navigation systems. St. Petersburg: Concern CSRI Elektropribor JSC; 2009. 278 p. (in Russian).
- 6. Black HD. A passive system for determining the attitude of a satellite. *AIAA Journal*. 1964;2(7):1350–1351. https://doi.org/10.2514/3.2555
- 7. Davenport PB. A vector approach to the algebra of rotations with applications. Washington, DC: National Aeronautics and Space Administration; 1968. 25 p.
- 8. Wu J, Zhou Z, Fourati H, Cheng Y. A super fast attitude determination algorithm for consumer-level accelerometer and magnetometer. *IEEE Transactions on Consumer Electronics*. 2018;64(3):375–381. https://doi.org/10.1109/TCE.2018.2859625

- 9. Zhou Z, Wu J, Wang J, Fourati H. Optimal, recursive and sub-optimal linear solutions to attitude determination from vector observations for GNSS/accelerometer/magnetometer orientation measurement. *Remote Sensing*. 2018;10(3):377. https://doi.org/10.3390/rs10030377
- 10. Valenti R, Dryanovski I, Xiao J. Keeping a good attitude: a quaternion-based orientation filter for IMUs and MARGs. *Sensors*. 2015;15(8):19302–19330. https://doi.org/10.3390/s150819302
- 11. Mahony R, Hamel T, Pflimlin J-M. Nonlinear complementary filters on the special orthogonal group. *IEEE Transactions on Automatic Control*. 2008;53(5):1203–1218. https://doi.org/10.1109/TAC.2008.923738
- 12. Madgwick SOH, Harrison AJL, Vaidyanathan R. Estimation of IMU and MARG orientation using a gradient descent algorithm. In: 2011 IEEE International Conference on Rehabilitation Robotics; 2011. p. 1–7. https://doi.org/10.1109/ICORR.2011.5975346
- 13. Kalman RE. A new approach to linear filtering and prediction problems. *Journal of Basic Engineering*. 1960;82(1):35–45. https://doi.org/10.1115/1.3662552
- 14. Hartikainen J, Solin A, Särkkä S. Optimal filtering with Kalman filters and smoothers. Espoo: Department of Biomedical Engineering and Computational Science, Aalto University School of Science; 2011. 150 p.
- 15. Open Source Sensor Fusion. An open source repository of algorithms and datasets for sensor fusion and analytics (Version 4.22 of Freescale Semiconductor's sensor fusion library). Available from: https://github.com/memsin-dustrygroup/Open-Source-Sensor-Fusion/tree/master [accessed 28 March 2025].
- 16. AHRS: Attitude and Heading Reference Systems. AHRS0.4.0 documentation. Available from: https://ahrs.readthedocs.io/en/latest/ [accessed 28 March 2025].
- 17. Bosch Sensortec. BNO055 intelligent 9-axis absolute orientation sensor. Reutlingen: Bosch Sensortec; 2014. Available from: https://www.bosch-sensortec.com/media/boschsensortec/downloads/datasheets/bst-bno055-ds000.pdf [accessed 28 March 2025].
- 18. Rainville E, Thomson J, Moulton M, Derakhti M. Measurements of nearshore ocean-surface kinematics through coherent arrays of free-drifting buoys. *Earth System Science Data*. 2023;15(11):5135–5151. https://doi.org/10.5194/essd-15-5135-2023
- 19. Feddersen F, Amador A, Pick K, et al. The wavedrifter: a low-cost IMU-based Lagrangian drifter to observe steepening and overturning of surface gravity waves and the transition to turbulence. *Coastal Engineering Journal*. 2024;66(1):44–57. https://doi.org/10.1080/21664250.2023.2238949
- 20. Veras Guimarães P, Ardhuin F, Sutherland P, et al. A surface kinematics buoy (SKIB) for wave—current interaction studies. *Ocean Science*. 2018;14(6):1449–1460. https://doi.org/10.5194/os-14-1449-2018
- 21. Crandle T, Cook M, Cook G, Celkis E. Advances in wave sensing using MEMS. In: Proceedings of OCEANS2016 MTS/IEEE Monterey; 2016. p. 1–4. https://doi.org/10.1109/OCEANS.2016.7761148
- 22. Tengberg A, Weiss G, Roach D. Directional wave, currents and environmental monitoring from navigation and hydrography buoys: an introduction to MOTUS. In: Proceedings of 2018 OCEANS MTS/IEEE Kobe Techno-Oceans (OTO); 2018. p. 1–10. https://doi.org/10.1109/OCEANSKOBE.2018.8559239
- 23. Zhou F, Zhang R, Zhang S. Measurement principle and technology of miniaturized strapdown inertial wave sensor. *Frontiers in Marine Science*. 2022;9:991996. https://doi.org/10.3389/fmars.2022.991996
- 24. InvenSense Inc. MPU-9250 product specification. Revision 1.1. San Jose: InvenSense Inc; 2016. Available from: www.invensense.com/wp-content/uploads/2015/02/PS-MPU-9250A-01-v1.1.pdf [accessed 28 March 2025].
- 25. Joosten H. Directional wave buoys and their elastic mooring. *International Ocean Systems*. 2006;10(4):18–21.
- 26. Bondur VG, Dulov VA, Murynin AB, Yurovsky YY. A study of sea-wave spectra in a wide wavelength range from satellite and in-situ data. *Izvestiya. Atmospheric and Oceanic Physics*. 2016;52(9):888–903. https://doi.org/10.1134/S0001433816090097
- 27. Fairall CW, Bradley EF, Hare JE, et al. Bulk parameterization of air—sea fluxes: updates and verification for the COARE algorithm. *Journal of Climate*. 2003;16(4):571—591. <a href="https://doi.org/10.1175/1520-0442(2003)016<0571">https://doi.org/10.1175/1520-0442(2003)016<0571: BPOASF>2.0.CO;2
- 28. Longuet-Higgins MS, Cartwright DE, Smith ND. Observations of the directional spectrum of sea waves using the motions of a floating buoy. In: Ocean wave spectra: proceedings of a conference. Englewood Cliffs: Prentice-Hall; 1961. p. 111–132.
- 29. Earle MD, Brown R, Baker DJ, McCall JC. Nondirectional and directional wave data analysis procedures. Stennis Space Center: NDBC; 1996. 43 p. (NDBC technical document 96–01). Available from: www.ndbc.noaa.gov/wavemeas.pdf [accessed 28 March 2025].
- 30. Young IR. The determination of confidence limits associated with estimates of the spectral peak frequency. *Ocean Engineering*. 1995;22(7):669–686. https://doi.org/10.1016/0029-8018(95)00002-3
- 31. Rossi GB, Nardone G, Settanta G, et al. Improvement in the post-processing of wave buoy data driven by the needs of a national coast and sea monitoring agency. *Sensors*. 2023;23(12):5371. https://doi.org/10.3390/s23125371

- 32. Yurovsky YY, Kudinov OB. Methods and errors of wave measurements using conventional inertial motion units. *Physical Oceanography*. 2025;32(1):63–83. Available from: http://physical-oceanography.ru/static/assets/files/2025/01/20250105.pdf [accessed 28 March 2025].
- 33. Pivaev P, Kudryavtsev V, Korinenko A, Malinovsky V. Field observations of breaking of dominant surface waves. *Remote Sensing*. 2021;13(16):3321. https://doi.org/10.3390/rs13163321

Литература

- 1. *Rabault J.*, *Nose T.*, *Hope G.* et al. OpenMetBuoy-v2021: An Easy-to-Build, Affordable, Customizable, Open-Source Instrument for Oceanographic Measurements of Drift and Waves in Sea Ice and the Open Ocean // Geosciences. 2022. Vol. 12, N 3. P. 110. EDN MCLHXX. https://doi.org/10.3390/geosciences12030110
- 2. *Collins C.O.*, *Dickhudt P.*, *Thomson J.* et al. Performance of moored GPS wave buoys // Coastal Engineering Journal. 2024. P. 1–27. EDN FOVQMW. https://doi.org/10.1080/21664250.2023.2295105
- 3. *Hope G.*, *Seldal T.I.*, *Rabault J.* et al. SFY-A Lightweight, High-Frequency, and Phase-Resolving Wave Buoy for Coastal Waters // Journal of Atmospheric and Oceanic Technology. 2025. Vol. 42, N 2. P. 133–154. EDN YF-PIDV.
- https://doi.org/10.1175/JTECH-D-23-0170.1
- 4. Грязин Д.Г. Расчет и проектирование буев для измерения морского волнения. СПб.: СПбГИТМО (ТУ), 2000. 134 с.
- 5. *Матвеев В.В.*, *Располов В.Я*. Основы построения бесплатформенных инерциальных навигационных систем. СПб.: ОАО Концерн ЦНИИ Электроприбор, 2009. 278 с.
- 6. *Black H.D.* A passive system for determining the attitude of a satellite // AIAA Journal. 1964. Vol. 2, N 7. P. 1350–1351. https://doi.org/10.2514/3.2555
- 7. *Davenport P.B.* A vector approach to the algebra of rotations with applications. National Aeronautics and Space Administration, 1968. 25 p.
- 8. Wu J., Zhou Z., Fourati H., Cheng Y. A Super Fast Attitude Determination Algorithm for Consumer-Level Accelerometer and Magnetometer // IEEE Transactions on Consumer Electronics. 2018. Vol. 64, N 3. P. 375—381. https://doi.org/10.1109/TCE.2018.2859625
- 9. *Zhou Z.*, *Wu J.*, *Wang J.*, *Fourati H.* Optimal, Recursive and Sub-Optimal Linear Solutions to Attitude Determination from Vector Observations for GNSS/Accelerometer/Magnetometer Orientation Measurement // Remote Sensing. 2018. Vol. 10, N 3. P. 377. EDN YGBQWL. https://doi.org/10.3390/rs10030377
- 10. *Valenti R.*, *Dryanovski I.*, *Xiao J.* Keeping a Good Attitude: A Quaternion-Based Orientation Filter for IMUs and MARGs // Sensors. 2015. Vol. 15, N 8. P. 19302–19330. https://doi.org/10.3390/s150819302
- 11. *Mahony R.*, *Hamel T.*, *Pflimlin J.-M.* Nonlinear Complementary Filters on the Special Orthogonal Group // IEEE Transactions on Automatic Control. 2008. Vol. 53, N 5. P. 1203–1218. https://doi.org/10.1109/TAC.2008.923738
- 12. *Madgwick S.O.H.*, *Harrison A.J.L.*, *Vaidyanathan R*. Estimation of IMU and MARG orientation using a gradient descent algorithm // 2011 IEEE International Conference on Rehabilitation Robotics. 2011. P. 1–7. https://doi.org/10.1109/ICORR.2011.5975346
- 13. *Kalman R.E.* A New Approach to Linear Filtering and Prediction Problems // Journal of Basic Engineering. 1960. Vol. 82, N 1. P. 35–45. https://doi.org/10.1115/1.3662552
- 14. *Hartikainen J.*, *Solin A.*, *Särkkä S.* Optimal filtering with Kalman filters and smoothers. Department of biomedica engineering and computational sciences, Aalto University School of Science, 2011. 150 p.
- 15. Open Source Sensor Fusion. An open source repository of algorithms and datasets for sensor fusion and analytics (Version 4.22 of Freescale Semiconductor's sensor fusion library). URL: https://github.com/memsindustrygroup/ Open-Source-Sensor-Fusion/tree/master (дата обращения: 28.03.2025).
- 16. AHRS: Attitude and Heading Reference Systems. AHRS0.4.0 documentation. URL: https://ahrs.readthedocs.io/en/latest/ (дата обращения: 28.03.2025).
- 17. Bosch Sensortec. BNO055 Intelligent 9-axis absolute orientation sensor. 2014. URL: https://www.bosch-sensortec.com/media/boschsensortec/downloads/datasheets/bst-bno055-ds000.pdf (дата обращения: 28.03.2025).
- 18. Rainville E., Thomson J., Moulton M., Derakhti M. Measurements of nearshore ocean-surface kinematics through coherent arrays of free-drifting buoys // Earth System Science Data. 2023. Vol. 15, N 11. P. 5135–5151. EDN HBBMLX. https://doi.org/10.5194/essd-15-5135-2023
- 19. *Feddersen F.*, *Amador A.*, *Pick K.* et al. The wavedrifter: a low-cost IMU-based Lagrangian drifter to observe steepening and overturning of surface gravity waves and the transition to turbulence // Coastal Engineering Journal. 2024. Vol. 66, No. 1. P. 44–57. EDN ZSVNKT. https://doi.org/10.1080/21664250.2023.2238949

- 20. *Veras Guimarães P.*, *Ardhuin F.*, *Sutherland P.* et al. A surface kinematics buoy (SKIB) for wave-current interaction studies // Ocean Science. 2018. Vol. 14, No. 6. P. 1449—1460. EDN GBSLNE. https://doi.org/10.5194/os-14-1449-2018
- 21. *Crandle T.*, *Cook M.*, *Cook G.*, *Celkis E.* Advances in wave sensing using MEMS // Proceedings of OCEANS2016 MTS/IEEE, Monterey. 2016. P. 1–4. https://doi.org/10.1109/OCEANS.2016.7761148
- 22. *Tengberg A.*, *Weiss G.*, *Roach D.* Directional wave, currents and environmental monitoring from navigation and hydrography buoys: An introduction to MOTUS // Proceedings of 2018 OCEANS MTS/IEEE Kobe Techno-Oceans (OTO). 2018. P. 1–10. https://doi.org/10.1109/OCEANSKOBE.2018.8559239
- 23. Zhou F., Zhang R., Zhang S. Measurement principle and technology of miniaturized strapdown inertial wavesensor // Frontiers in Marine Science. 2022. Vol. 9. 991996. EDN OIQFGM. https://doi.org/10.3389/fmars.2022.991996
- 24. InvenSense[™], Inc. MPU-9250 product specification. Revision 1.1. 2016. URL: www.invensense.com/wp-content/uploads/2015/02/PS-MPU-9250A-01-v1.1.pdf (дата обращения: 28.03.2025).
- 25. *Joosten H.* Directional wave buoys and their elastic mooring // International Ocean Systems. 2006. Vol. 10, N 4. P. 18–21.
- 26. Bondur V.G., Dulov V.A., Murynin A.B., Yurovsky Yu. Yu. A study of sea-wave spectra in a wide wavelength range from satellite and in-situ data // Izvestiya. Atmospheric and Oceanic Physics. 2016. Vol. 52, N 9. P. 888–903. EDN YVCIWH. https://doi.org/10.1134/S0001433816090097
- 27. Fairall C.W., Bradley E.F., Hare J.E. et al. Bulk Parameterization of Air-Sea Fluxes: Updates and Verification for the COARE Algorithm // Journal of Climate. 2003. Vol. 16, N4. P. 571–591. <0571: BPOASF>2.0.CO;2. EDN LZCPGF. https://doi.org/10.1175/1520-0442(2003)016
- 28. Longuet-Higgins M.S., Cartwright D.E., Smith N.D. Observations of the directional spectrum of sea waves using the motions of a floating buoy // Ocean wave spectra: Proceedings of a conference, N.A.O. Sciences, ed., Prentice-Hall. 1961. P. 111–132.
- 29. Earle M.D., Brown R., Baker D.J., McCall J.C. Nondirectional and directional wave data analysis procedures. Stennis Space Center, 1996. 43 p. (NDBC technical document 96–01). URL: www.ndbc.noaa.gov/wavemeas.pdf (дата обращения: 28.03.2025).
- 30. *Young I.R.* The determination of confidence limits associated with estimates of the spectral peak frequency // Ocean Engineering. 1995. Vol. 22, N 7. P. 669–686. https://doi.org/10.1016/0029-8018(95)00002-3
- 31. *Rossi G.B.*, *Nardone G.*, *Settanta G.* et al. Improvement in the Post-Processing of Wave Buoy Data Driven by the Needs of a National Coast and Sea Monitoring Agency // Sensors. 2023. Vol. 23, N 12. P. 5371. EDN CIYKPI. https://doi.org/10.3390/s23125371
- 32. *Yurovsky Yu. Yu.*, *Kudinov O.B.* Methods and Errors of Wave Measurements Using Conventional Inertial Motion Units // Physical Oceanography. 2025. Vol. 32, N 1. P. 63–83. EDN WTGOVI
- 33. *Pivaev P., Kudryavtsev V., Korinenko A., Malinovsky V.* Field Observations of Breaking of Dominant Surface Waves// Remote Sensing. 2021. Vol. 13, N 16. P. 3321. EDN NMQQBA. https://doi.org/10.3390/rs13163321

About the Author

- Yury Yu. YUROVSKY Leading Researcher, Head of Laboratory, MHI RAS, CandSc. (Phys.-Math.), ORCID: 0000-0002-9995-3965, WoS ResearcherID: F-8907—2014, Scopus AuthorID: 24377122700, SPIN-code (РИНЦ): 8482-5777, e-mail: y.yurovsky@mhi-ras.ru
- Oleg B. KUDINOV, Researcher, Head of Laboratory, MHI RAS, CandSc. (Tech.), Scopus AuthorID: 57201072321, SPIN-code (РИНЦ): 2248-7034, e-mail: obk91@mail.ru